J Mater Sci (2014) 49:2263–2269
DOI 10.1007/s10853-013-7922-4

Reduced graphene oxide and CdTe nanoparticles co-decorated TiO_2 nanotube array as a visible light photocatalyst

Meijun Liu · Lei He · Xuanneng Liu · Chengbin Liu · Shenglian Luo

Received: 28 October 2013 / Accepted: 25 November 2013 / Published online: 6 December 2013

Abstract TiO_2 nanotube array (TiO_2 NT) was co-decorated by reduced graphene oxide (RGO) and CdTe nanoparticles (NPs) through a simple one-step electrodeposition process. RGO film was formed on the top surface of TiO_2 NT and CdTe NPs homogeneously dispersed within the RGO sheets and on the inner/outer walls of TiO_2 NT. Resulting from the synergetic effect of RGO and CdTe, the photocatalytic activity of the ternary RGO/CdTe–TiO_2 NT photocatalyst far exceeded those of bare TiO_2 NT, RGO-TiO_2 NT, and CdTe–TiO_2 NT photocatalysts in the degradation of herbicide 2,4-dichlorophenoxyacetic acid (2,4-D) under simulated solar light or visible light irradiation. After 180-min UV–Vis (or visible light) irradiation, almost 100 % (or 96 %) 2,4-D removal efficiency was achieved on RGO/CdTe–TiO_2 NT, much higher than 42 % (or 2 %) on bare TiO_2 NT, 58 % (or 10 %) on RGO–TiO_2 NT, and 52 % (or 41 %) on CdTe–TiO_2 NT. This study will inspire better design of advanced photocatalysts with high visible-light photocatalytic activity.

Introduction

Among all the investigated TiO_2 nanostructured materials, TiO_2 nanotube array vertically oriented on a Ti-foil, has been paid particular attention [1, 2] because of the large interfacial area, excellent electron percolation pathways, and especially the excellent reusability relative to other powdery TiO_2 nanomaterials. However, the wide band gap (3.2 eV) restricts the photoresponse of TiO_2 to only ultraviolet region with the wavelength below 390 nm of the solar spectrum and depresses vastly utilization ratio of solar power. In order to extend the optical absorption into the visible-light region, various strategies have been designed, including doping TiO_2 with metals or nonmetals [3, 4] and coupling TiO_2 with narrow bandgap semiconductors such as CdS [5, 6], CdSe [7, 8], PbS [9, 10], Cu_2O [11, 12], and so on. Besides, the photogenerated electron–hole pairs that are responsible for chemical reactions with pollutants tend to quick recombination, leading to decreased efficiency in the photocatalytic activity of TiO_2. The narrow bandgap semiconductors coupled TiO_2 photocatalysts show extended absorption from UV to visible region and also enhanced photoinduced electron–hole separation occurring at the heterojunction interface between semiconductors [13], thus improving the efficiency of the photocatalytic reaction. TiO_2 nanotube arrays have been previously used as substrates for constructing highly efficient TiO_2-based hybrids for photocatalysis [4, 9].

CdTe has shown considerable promise for building thin film solar cells capable of a significant light to electricity conversion efficiency owing to its nearly ideal bandgap for solar terrestrial photoconversion (1.5 eV) and its high absorption coefficient [14, 15].To date, most studies on CdTe have involved in solar cells [16, 17] and sensors [18, 19]. Few studies on photocatalysis have been reported [20]. To the best of our knowledge, the combination of CdTe and graphene has been not reported in photocatalysis.

Graphene, a one-atom-thick planar sheet of sp^2-hybridized carbon atoms, has attracted strong scientific and technological attentions in various fields including photocatalysis [21, 22]. The graphene material owns excellent electron capture and transport properties [23, 24], large

M. Liu · L. He · X. Liu · C. Liu (✉) · S. Luo
State Key Laboratory of Chemo/Biosensing and Chemometrics, Hunan University, Changsha 410082, People's Republic of China
e-mail: chem_cbliu@hnu.edu.cn

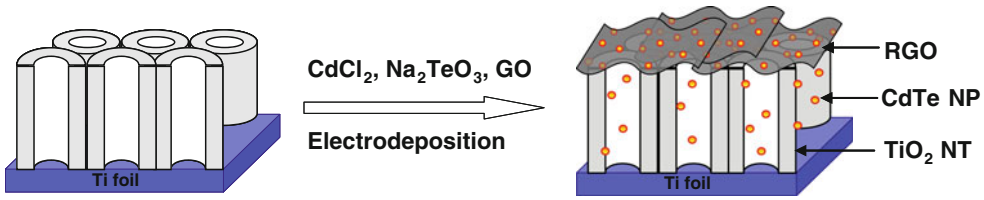

Scheme 1 Schematic illustration of one-step electrochemical preparation of RGO/CdTe–TiO_2 NT

specific surface area [25], and good affinity toward organic molecules [26–28]. Our recent studies reveal that TiO_2 NT modified with graphene show high performance in photocatalytic degradation of organic pollutants [21, 29].

In the present work, a simple one-step electrodeposition method is proposed for the simultaneous fabrication of reduced graphene oxide (RGO) and CdTe nanoparticles (NPs) on TiO_2 NT (Scheme 1). The distinctive advantage of using n-type TiO_2 and p-type CdTe to form a p–n heterojunction is that it not only increases junction areas but also promotes unidirectional charge transport due to the one-dimensional features of the tubes. The degradation of herbicide 2,4-dichlorophenoxyacetic acid (2,4-D) on the advanced RGO/CdTe–TiO_2 NT photocatalyst was investigated. 2,4-D, a model pollutant, has drawn considerable attention in photocatalytic degradation recently, considering that it is a typical widely used and highly toxic synthetic phytohormone.

Experimental

Chemicals and materials

Titanium foil (99.8 %, 250 μm thickness) was purchased from Aldrich (Milwaukee, WI, USA), 2,4-D was obtained from Shanghai JieHui biological technology Co. Ltd., and graphite powder about 50 mm was purchased from Shanghai Carbon Co., Ltd. Cadmium chloride ($CdCl_2$), sodium tellurite (Na_2TeO_3), and other reagents are of analytical grade and are all used as received. Deionized water was used for preparation of all aqueous solutions.

Preparation of TiO_2 NT

TiO_2 nanotube array (TiO_2 NT) was prepared according to our previous work [30]. Prior to anodization, titanium foils were ultrasonically cleaned successively in acetone and ethanol. The cleaned foil was anodized at 15 V in an electrolyte containing 0.1 M NaF and 0.5 M $NaHSO_4$ at room temperature for 3 h. The anodizing cell was a two-electrode system using a platinum as the counter electrode, resulting in the TiO_2 NTs with a pore size of 90–100 nm, a length of 320 nm and an efficient electrode area of 3 cm × 1 cm on each side. The as-anodized TiO_2 NTs were sintered in oxygen atmosphere at 500 °C for 3 h with heating and cooling rate of 2 °C min^{-1}.

Preparation of RGO/CdTe–TiO_2 NT

Graphite oxide was initially prepared from graphite powder according to the Hummers method [31]. After rinsing and drying, the synthesized graphite oxide powder was then exfoliated in a 0.1 M, pH 4.0 citric acid–sodium citrate buffer solution (CBS) by ultrasonication for 3 h to obtain a stable yellow-brown graphene oxide (GO) colloidal dispersion (0.4 mg mL^{-1}).

To electrodeposit RGO and CdTe nanoparticles on TiO_2 NT, a 0.1 M, pH 4.0 CBS containing 0.4 mg mL^{-1} GO, 0.05 mol L^{-1} $CdCl_2$, and 0.025 mol L^{-1} Na_2TeO_3 was prepared as the electrolyte. The impulse electrochemical deposition was carried out at a potential of −2.0 V for 0.2 s, and then a potential of −0.00001 V for 1 s, with optimized 100 pulse sequences in a standard three-electrode system using the annealed TiO_2 NT/Ti foil as the working electrode, a Pt-foil as the counter electrode and saturated calomel electrode (SCE) as the reference electrode, on an electrochemical workstation (IM6ex, Zahner Elektrik, Germany). After deposition, the working electrodes were rinsed with deionized water, and then dried at room temperature to get RGO/CdTe–TiO_2 NT.

Meanwhile, TiO_2 NT/Ti foils decorated with only RGO film or CdTe NPs for reference were fabricated separately following the same procedure just using their respective precursors (0.4 mg mL^{-1} GO in 0.1 M, pH 4.0 CBS for RGO–TiO_2 NT preparation, and 0.05 mol L^{-1} $CdCl_2$ and 0.025 mol L^{-1} Na_2TeO_3 in 0.1 M, pH 4.0 CBS for CdTe–TiO_2 NT preparation).

Characterization

The morphologies of the products were characterized by a Model S-4800 field emission scanning electron microscope (FESEM). Energy dispersive X-ray (EDX) spectrometer fitted to the electron microscope was applied for elemental analysis. The crystal phases of the resulting samples were determined by an X-ray diffractometer with Cu–K_α radiation (XRD, M21X, MAC Science Ltd., Japan). UV–Vis

diffuse reflectance spectra (DRS) were recorded with a UV–Visible spectrophotometer (Cary 300, USA) equipped with an integrating sphere with radius of 150 mm.

Photocurrent measurements

Photocurrents were recorded on a CHI 660D electrochemical workstation by using a three-electrode configuration with bare TiO_2 NT or the modified TiO_2 NT/Ti sheet as the working electrode, a Pt-foil as the counter electrode and an SCE as the reference electrode in 0.5 M Na_2SO_4 solution. A 500 W xenon arc lamp (CHF–XQ–500 W, Beijing Changtuo Co., Ltd.) served as the simulated solar light source (280–2000 nm) with the photon flux of 100 mW cm^{-2} measured by NOVA Oriel 70260 with a thermodetector.

Photocatalytic degradation of 2,4-D

The photocatalytic degradation experiments were carried out under stirring in a quartz beaker containing 60 mL 10 mg L^{-1} 2,4-D. The photocatalyst samples with a total active area of 6.0 cm^2 were vertically placed in the quartz beaker. A 500 W xenon arc lamp (CHF–XQ–500 W, Beijing Changtuo Co., Ltd.), with the photon flux of 100 mW cm^{-2} served as the light source to simulate solar light irradiation or visible light irradiation (with a UV-cutoff filter $\geq$420 nm). Before the irradiation, the system was maintained in the dark for 0.5 h to reach complete adsorption–desorption equilibrium, so that the decreased concentration of 2,4-D with irradiation time can fully reflect the photocatalytic activities of the catalysts. The concentration of 2,4-D was determined by UV–Vis spectrophotometry on a Cary 300 spectrophotometer (Varian) according to the characteristic absorbance of 227 nm. The accurate concentration of 2,4-D was determined by high-performance liquid chromatography (HPLC, Agilent 1100HPLC).

Results and discussion

Morphology and structure characterization

The surface morphologies of the prepared photocatalysts are shown in Fig. 1. The bare TiO_2 NT is composed of high-density, well-ordered, and uniform TiO_2 nanotubes in pore size of about 90 nm (Fig. 1a). After deposition of GO onto the TiO_2 NT/Ti electrode, a continuous and transparent RGO film was formed on the top surface of TiO_2 NT (Fig. 1b). It should be noted that the electrochemical reduction of GO has been well documented in our previous work [21]. Figure 1c shows that the CdTe NPs were distributed on the outside and inside walls of TiO_2 NT, where the CdTe NPs seriously aggregated. The one-pot deposition of RGO and CdTe led to the homogeneous dispersion of CdTe NPs with smaller size within RGO sheets and inner/outer walls of TiO_2 NT (Fig. 1d). As we know, homogeneous and small particles are more favorable for light absorption and electrons transport [32].

The composition and structure of the RGO/CdTe–TiO_2 NT were confirmed by EDX and XRD analysis. The EDX results demonstrate that the atom ratio of Te and Cd was 1.05, proximal to the intrinsic molar component of CdTe. Figure 2 shows the XRD spectra of bare TiO_2 NT (Fig. 2a) and RGO/CdTe–TiO_2 NT (Fig. 2b). Besides the peaks coming from Ti substrate (JCPDS file No. 05-0682, marked by Ti), all the samples exhibited the characteristic diffraction peaks of anatase TiO_2 NTs (JCPDS file No. 71-1167, marked by A). The similar XRD patterns indicate that the deposition of RGO or/and CdTe had no influence on the crystalline structure of the TiO_2 NT. There was no obvious diffraction peak of graphene in the RGO/CdTe–TiO_2 NT due to the two-dimensional thin-film structure of graphene that could not be detected by conventional powder X-ray diffractometer. By comparison of RGO/CdTe–TiO_2 NT with bare TiO_2 NT, some new peaks (marked by C) appeared which were assigned to cubic crystalline CdTe according to JCPDS file No. 89-3053. Figure 3 gives the Raman spectra of GO and RGO. The ratio of D-band to G-band significantly enhanced after GO had been deposited onto the surface of TiO_2 NT, meaning the reduction of GO into RGO. This is well consistent with the literature [9].

Property characterization

It is well known that for elimination of environmental pollutants, an effective photocatalyst should possess a high photocatalytic activity both in UV and visible region, so that the whole solar-energy spectrum can be used as much as possible. The DRS spectra of RGO/CdTe–TiO_2 NT and other samples were shown in Fig. 4. The bare TiO_2 NT exhibits two absorption edges at about 420 and 540 nm attributed to intrinsic band-gap absorption of TiO_2 and structural defect absorption, respectively [33]. It is clear to be seen that the modification with RGO or CdTe resulted in red shifts in the absorption edges, and moreover the absorption intensities significantly increased in the whole UV–Vis region. Further enhanced UV–Vis light absorption occurred on the ternary RGO/CdTe–TiO_2 NT photocatalyst, due to the synergetic effect of CdTe and RGO.

The photoinduced charge separation in the photocatalysts was then evaluated by measuring the photocurrent. Figure 5 shows the current–time (*I–t*) characteristics of the bare TiO_2 NT and modified-TiO_2 NT electrodes recorded

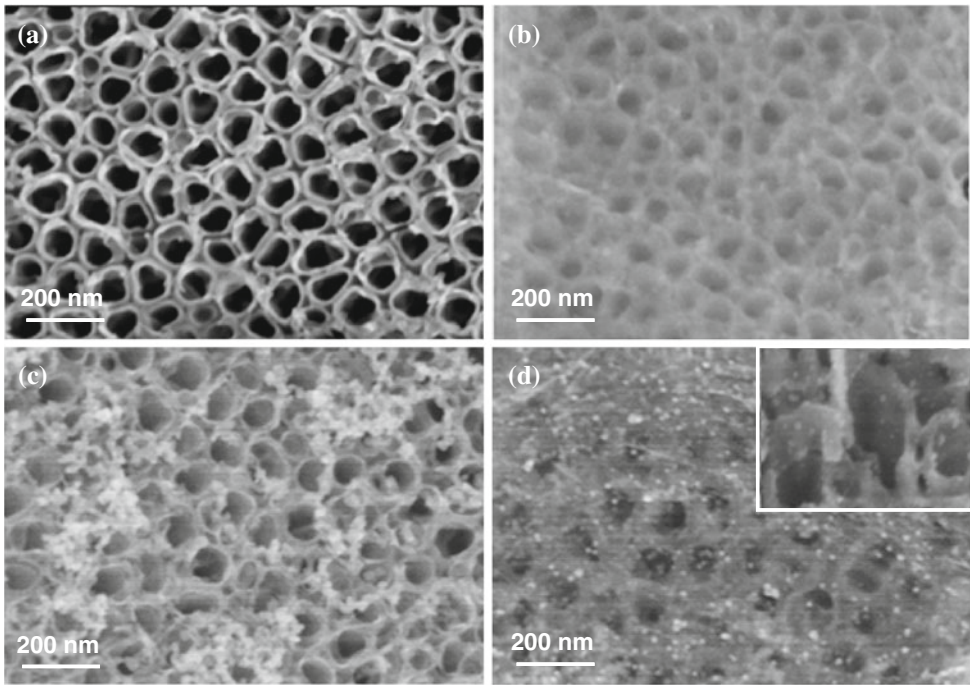

Fig. 1 SEM images of **a** bare TiO_2 NT, **b** RGO–TiO_2 NT, **c** CdTe–TiO_2 NT, and **d** RGO/CdTe–TiO_2 NT

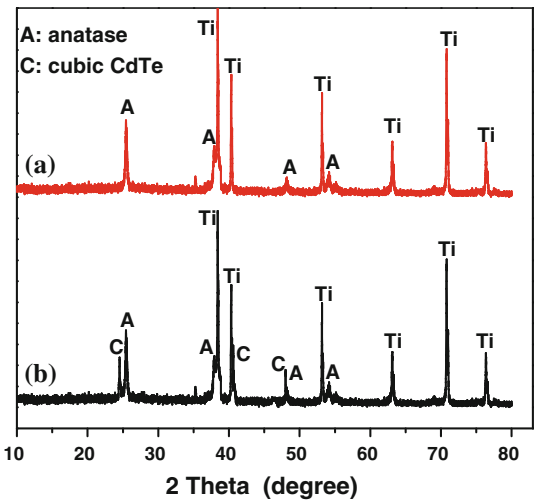

Fig. 2 XRD patterns of **a** bare TiO_2 NT and **b** RGO/CdTe–TiO_2 NT

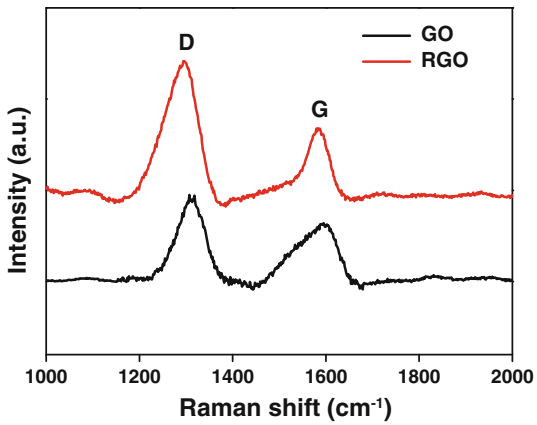

Fig. 3 Raman spectra of GO and RGO

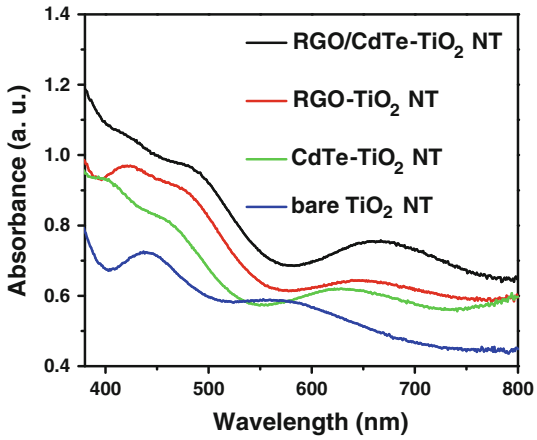

Fig. 4 DRS spectra of bare TiO_2 NT, RGO–TiO_2 NT, CdTe–TiO_2 NT, and RGO/CdTe–TiO_2 NT

in 0.5 M Na_2SO_4. Both RGO–TiO_2 NT (Fig. 5b) and CdTe–TiO_2 NT (Fig. 5c) displayed much increased photocurrent responses in comparison with bare TiO_2 NT (Fig. 5a), indicating more photogenerated charges which were effectively separated in RGO–TiO_2 NT and CdTe–TiO_2 NT. As reported, the calculated work function for RGO is 4.7–4.9 eV [34], facilitating the fast capture of electrons from TiO_2 with a conduction band level of about −4.2 eV (vs vacuum). The CdTe–TiO_2 NT hybrid showed higher photocurrent density than RGO–TiO_2 NT because of the simultaneous excitations of the two semiconductors under UV–Vis irradiation in the former that produced more electron–hole pairs relative to only TiO_2 excitation in the

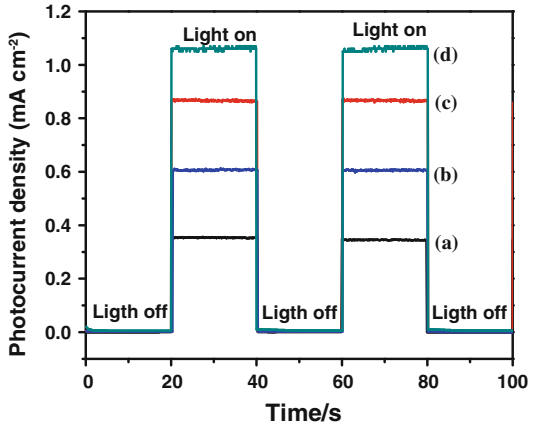

Fig. 5 Photocurrent responses of *a* bare TiO_2 NT, *b* RGO–TiO_2 NT, *c* CdTe–TiO_2 NT, and *d* RGO/CdTe–TiO_2 NT in 0.5 M Na_2SO_4 solution under simulated solar light (100 mW cm^{-2}) irradiation with a bias of 0 V (vs SCE)

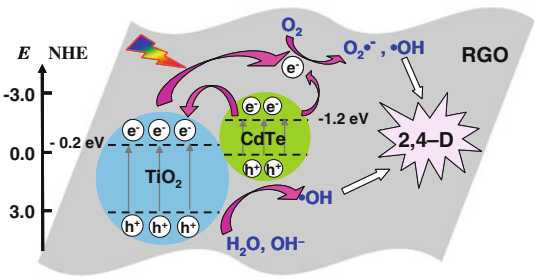

Scheme 2 Illustration of charge transfer in RGO/CdTe–TiO_2 NT and the formation of photocatalytically active species for degradation of 2,4-D

latter. By incorporation of RGO into CdTe–TiO_2 NT to form ternary RGO/CdTe–TiO_2 NT, the photocurrent density further increased (Fig. 5d) because of more effective transfer and separation of the photoinduced charges between the RGO/TiO_2 and RGO/CdTe heterojunction interfaces according to the band alignment between CdTe and TiO_2, where the photoexcited electrons transfer from the conduction band (CB) of CdTe to the CB of TiO_2 [20], then to RGO and finally to RGO (Scheme 2).

Adsorption capacity of photocatalysts toward 2,4-D

The adsorption capacity was investigated by placing the photocatalysts in a 10 mL 1.0 mg L^{-1} (4.5 μM) 2,4-D aqueous solution for 2 h and evaluating the remaining 2,4-D concentration by HPLC. Adsorptivity of catalysts is a crucial factor required for efficient degradation of pollutant molecules particularly in a low concentration level. One of the prominent advantages of graphene over other traditional materials, such as semiconductors, noble metals, and dyes for modification of TiO_2, is its high affinity toward organic molecules, especially aromatic molecules [26].

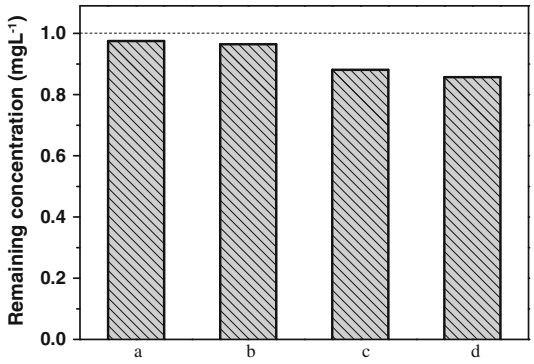

Fig. 6 Adsorption of 2,4-D on: *a* bare TiO_2 NT, *b* CdTe–TiO_2 NT, *c* RGO–TiO_2 NT, and *d* RGO/CdTe–TiO_2 NT

Herein, although the RGO layer deposited on the surface of TiO_2 NT blocked the tube entrance and perhaps decreased the effective area of TiO_2 NT, about 13 % of the 2,4-D molecules were adsorbed on RGO–TiO_2 NT (Fig. 6c), far higher than 2 % on bare TiO_2 NT (Fig. 6a). This indicates that the nominally large specific surface of TiO_2 NT played a minor role in adsorbing 2,4-D due to its high hydrophilicity and the π–π and/or hydrophobic interactions between RGO and 2,4-D were responsible for the good adsorptivity of RGO–TiO_2 NT. Apparently, CdTe NPs incorporation had no significantly positive effect on the adsorptivity by comparison of CdTe–TiO_2 NT (Fig. 6b) and RGO/CdTe–TiO_2 NT (Fig. 5d) with bare TiO_2 NT (Fig. 6a) and RGO–TiO_2 NT (Fig. 6c), respectively.

Subsequently, the photocatalysts with adsorbed 2,4-D were irradiated with a 500 W xenon arc lamp for 30 min, and then the catalysts were repeatedly rinsed with a sodium hydroxide solution. It was shown that no 2,4-D was detected in the condensed eluent, implying that the absorbed 2,4-D had been effectively degraded. This result means that RGO could extract 2,4-D molecules from solution and then concentrate them near the catalyst surface to promote the photocatalytic degradation.

Degradation of 2,4-D

Figure 7 shows the photocatalytic degradation results of 2,4-D over the photocatalysts under UV–Vis light irradiation (Fig. 7a) and visible light irradiation (Fig. 7b). Under UV–Vis light irradiation, bare TiO_2 NT, CdTe–TiO_2 NT, and RGO–TiO_2 NT showed moderate photocatalytic activities. After 180-min UV–Vis irradiation, only 42, 52, and 58 % removal of 2,4-D over bare TiO_2 NT, CdTe–TiO_2 NT, and RGO–TiO_2 NT were observed, respectively, while almost 100 % removal of 2,4-D over RGO/CdTe–TiO_2 NT was achieved. The result should be attributed to the simultaneous excitations of CdTe and TiO_2 under UV–Vis irradiation, the excellent electron capture and transport

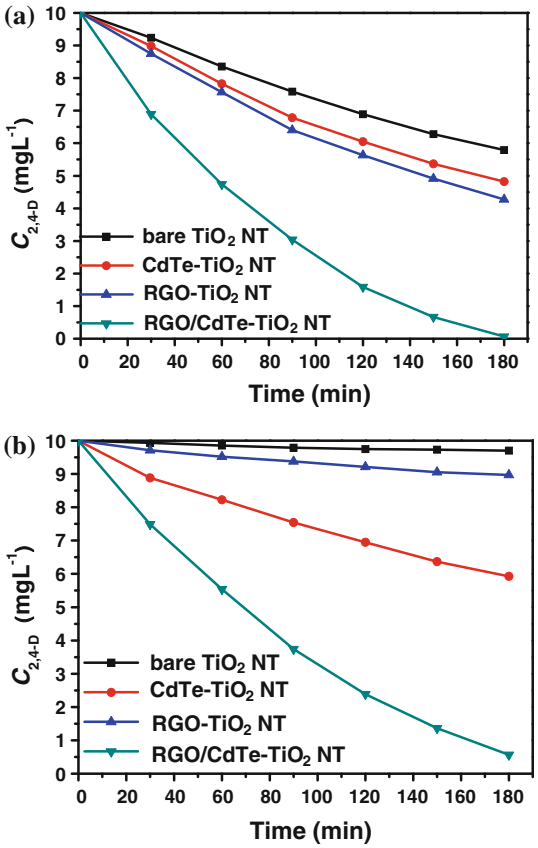

Fig. 7 Photocatalytic degradation of 2,4-D over the photocatalysts under **a** UV–Vis light irradiation and **b** visible light irradiation. The initial 2,4-D concentration is 10.0 mg L^{-1}

properties, and good adsorption capacity of RGO. Under visible light irradiation, only CdTe was excited, so both CdTe–TiO_2 NT and RGO/CdTe–TiO_2 NT exhibited obvious photocatalytic activities while other photocatalyst without CdTe showed negative photocatalytic activities. Furthermore, it is clearly seen that RGO/CdTe–TiO_2 NT showed about 96 % degradation efficiency of 2,4-D much higher than 41 % on CdTe–TiO_2 NT after 180-min irradiation, indicative of a synergetic effect among RGO, CdTe, and TiO_2. As mentioned in photocurrent analysis, the photogenerated electrons could transfer from CdTe to TiO_2, TiO_2 to RGO, and CdTe to RGO (Scheme 2), facilitating the maximum photoinduced charge separation in RGO/CdTe–TiO_2 NT.

Conclusion

TiO_2 NT co-modified with reduced graphene oxide (RGO) and CdTe NPs was prepared using a simple one-step electrodeposition technique. As usual, the narrow-band-gap CdTe sensitized the TiO_2 NT to extend its absorption from UV to visible region and enhanced the photogenerated electron–hole separation in the photocatalyst. Furthermore, the effects were greatly aggrandized by introduction of the excellent electron acceptor and transporter RGO which effectively collected the excited electrons from both CdTe and TiO_2 and then dispatched them to reaction sites, resulting in the enhanced photocatalytic activity. This study will inspire better design of advanced photocatalysts with high UV–Visible-light photocatalytic activity.

Acknowledgements This work was supported by Excellent Youth Foundation of Hunan Scientific Committee (14JJ1015), the National Natural Science Foundation of China (51178173, 51202065, J1210040, and J1103312), and Program for Innovation Research Team in University (IRT1238).

References

1. Ryu J, Lee SH, Nam DH, Park CB (2011) Rational design and engineering of quantum-dot sensitized titanium dioxide nanotube arrays for artificial photosynthesis. Adv Mater 23:1883–1888
2. Allam NK, Shankar K, Grimes CA (2008) Photoelectrochemical and water photoelectrolysis properties of ordered TiO_2 nanotubes fabricated by Ti anodization in fluoride-free HCl electrolytes. J Mater Chem 18:2341–2348
3. Khan MA, Yang OB (2009) Photocatalytic water splitting for hydrogen production under visible lighton Ir and Co ionized titanian anotube. Catal Today 146:177–182
4. Luo SL, Xiao Y, Yang L, Liu CB, Su F, Li Y, Cai Q, Zeng G (2011) Simultaneous detoxification of hexavalent chromium and acid orange 7 by a novel Au/TiO_2 heterojunction composite nanotube arrays. Sep Purif Technol 79:85–91
5. Shao ZB, Zhu W, Li Z, Yang Q, Wang G (2012) One-step fabrication of CdS nanoparticle-sensitized TiO_2 nanotube arrays via electrodeposition. J Phys Chem C 116:2438–2442
6. Baker DR, Kamat PV (2009) Photosensitization of TiO_2 nanostructures with CdS quantum dots: particulate versus tubular support architectures. Adv Funct Mater 19:805–811
7. Kongkanand A, Tvrdy K, Takechi K, Kuno M, Kamat PV (2008) J Am Chem Soc 130:4007
8. Zhang H, Quan X, Chen S, Yu HT, Ma N (2009) "Mulberry-like" CdSe nanoclusters anchored on TiO_2 nanotube arrays: a novel architecture with remarkable photoelectrochemical performance. Chem Mater 21:3090–3095
9. Zhang X, Tang Y, Li Y, Wang Y, Liu X, Liu CB, Luo SL (2013) Reduced graphene oxide and PbS nanoparticles co-modified TiO_2 nanotube arrays as a recyclable and stable photocatalyst for efficient degradation of pentachlorophenol. Appl Catal A 457:78–84
10. Ratanatawanate C, Tao Y, Balkus KJ (2009) Photocatalytic activity of PbS quantum dot/TiO_2 nanotube composites. J Phys Chem C 113:10755–10760
11. Yang L, Luo SL, Li Y, Xiao Y, Kang Q, Cai QY (2010) High efficient photocatalytic degradation of p-nitrophenol on a unique Cu_2O/TiO_2 p–n heterojunction network catalyst. Environ Sci Technol 44(19):7641–7646
12. Hou Y, Li XY, Zou XJ, Quan X, Chen GH (2009) Photoeletrocatalytic activity of a Cu_2O-loaded self-organized highly oriented TiO_2 nanotube array electrode for 4-chlorophenol degradation. Environ Sci Technol 43:858–863
13. Bessekhouad Y, Robert D, Weber JV (2005) Photocatalytic activity of Cu_2O/TiO_2, Bi_2O_3/TiO_2 and $ZnMn_2O_4/TiO_2$ heterojunctions. Catal Today 101:315–321

14. Birkmire RW, Eser E (1997) Polycrystalline thin film solar cells: present status and future potential. Annu Rev Mater Sci 27:625–653
15. Chu TL, Chu SS (1995) Thin film II–VI photovoltaics. Solid State Electron 38:533–549
16. Bi H, Huang Fu, Liang, Xie X, Jiang M (2011) Transparent conductive graphene films synthesized by ambient pressure chemical vapor deposition used as the front electrode of CdTe solar cells. Adv Mater 23(28):3202–3206
17. Han J, Spanheimer C, Haindl G, Fu G, Krishnakumar V, Schaffner J, Fan C, Zhao K, Klein A, Jaegermann W (2011) Optimized chemical bath deposited CdS layers for the improvement of CdTe solar cells. Sol Energy Mater Sol C 95(3):816–820
18. Chen Y, Chen Z, He Y, Lin H, Sheng P, Liu C, Luo S, Cai Q (2010) L-cysteine-capped CdTe QD-based sensor for simple and selective detection of trinitrotoluene. Nanotechnology 21:125502–125506
19. Ma Q, Cui H, Su X (2009) Highly sensitive gaseous formaldehyde sensor with CdTe quantum dots multilayer films. Biosens Bioelectron 25(4):839–844
20. Seabold JA, Shankar K, Wilke RHT, Paulose M, Varghese OK, Grimes CA, Choi KS (2008) Photoelectrochemical properties of heterojunction CdTe/TiO_2 electrodes constructed using highly ordered TiO_2 nanotube arrays. Chem Mater 20(16):5266–5273
21. Liu CB, Teng Y, Liu R, Luo SL, Tang YH, Chen L, Cai Q (2011) Fabrication of graphene films on TiO_2 nanotube arrays for photocatalytic application. Carbon 49:5312–5320
22. Zhang H, Lv X, Li Y, Wang Y, Li J (2010) P25-graphene composite as a high performance photocatalyst. ACS Nano 4:380–386
23. Lightcap IV, Kosel TH, Kamat PV (2010) Anchoring semiconductor and metal nanoparticles on a two-dimensional catalyst mat. Storing and shuttling electrons with reduced graphene oxide. Nano Lett 10:577–583
24. Geng JX, Jung HT (2010) Porphyrin functionalized graphene Sheets in aqueous suspensions: from the preparation of graphene sheets to highly conductive graphene films. J Phys Chem C 114(18):8227–8234
25. Stoller MD, Park S, Zhu Y, An J, Ruoff RS (2008) Graphene-based ultracapacitors. Nano Lett 8:3498–3502
26. Englert JM, Röhrl J, Schmidt CD, Graupner R, Hundhausen M, Hauke F, Hirsch A (2009) Soluble graphene: generation of aqueous graphene solutions aided by a perylenebisimide-based bolaamphiphile. Adv Mater 21:4265–4269
27. Geng JX, Kong BS, Yang SB, Jung HT (2010) Preparation of graphene relying on porphyrin exfoliation of graphite. Chem Commun 46:5091–5093
28. Sun JH, Xiao LH, Meng DL, Geng JX, Huang Y (2013) Enhanced photoresponse of large-sized photoactive graphene composite films based on water-soluble conjugated polymers. Chem Commun 49:5538–5540
29. Liu X, Tang YH, Luo SL, Wang Y, Zhang X, Chen Y, Liu CB (2013) Reduced graphene oxide and $CuInS_2$ co-decorated TiO_2 nanotube arrays for efficient removal of herbicide 2,4-dichlorophenoxyacetic acid from water. J Photoch Photobio A 262:22–27
30. Liu Y, Liu R, Liu CB, Luo SL, Yang L, Sui F, Teng Y, Yang R, Cai Q (2010) Enhanced photocatalysis on TiO_2 nanotube arrays modified with molecularly imprinted TiO_2 thin film. J Hazard Mater 182:912–918
31. Hummers WS Jr, Offeman RE (1958) Preparation of graphitic oxide. J Am Chem Soc 80(6):1339
32. Jassby D, Budarz JF, Wiesner M (2012) Impact of aggregate size and structure on the photocatalytic properties of TiO_2 and ZnO nanoparticles. Environ Sci Technol 46(13):6934–6941
33. Yang L, Luo SL, Liu R, Cai Q, Xiao Y, Liu S, Su F, Wen L (2010) Fabrication of CdSe nanoparticles sensitized long TiO_2 nanotube arrays for photocatalytic degradation of anthracene-9-carbonxylic acid under green monochromatic light. J Phys Chem C 114(11):4783–4789
34. Pang S, Tsao HN, Feng X, Müllen K (2009) Patterned graphene electrodes from solution-processed graphite oxide films for organic field-effect transistors. Adv Mater 21:3488–3491